

Vorticity probes and the characterization of vortices in the Kelvin–Helmholtz instability in the large plasma device experiment

W. Horton^{a)} and Jean C. Perez^{b)}

Institute for Fusion Studies, University of Texas at Austin, Austin, Texas 78712

Troy Carter^{c)}

Department of Physics and Astronomy, University of California, Los Angeles, California 90095

Roger Bengtson^{d)}

Fusion Research Center, University of Texas at Austin, Austin, Texas 78712

(Received 9 June 2004; accepted 4 October 2004; published online 7 January 2005)

A new five-pin probe design called the vorticity probe is presented that explicitly measures the vorticity in the $\mathbf{E} \times \mathbf{B}$ flow from floating potentials, independent of any absolute calibration errors. The five Tantalum probe tips are arranged in a diamond pattern with 5 mm tip spacing. The fluctuating floating potential at each tip is measured and used to compute a finite-difference approximation of the $\mathbf{E} \times \mathbf{B}$ vorticity. The probe is tested in the large plasma device (LAPD) [W. Gekelman *et al.*, *Rev. Sci. Instrum.* **62**, 2875 (1991)], operated with a variable bias between the anode and the chamber wall that creates a sharply localized E_r profile at 30 cm from the axis of the 100 cm diameter chamber. The fluctuations are peaked in the shear flow layer and are correlated with theoretical calculations of the Kelvin–Helmholtz instability for this plasma. The spectrum at 15–30 kHz matches the theoretical prediction from the measured dE_r/dr gradient that reaches 17 kV/m² in the $B=0.075$ T axial magnetic field. © 2005 American Institute of Physics. [DOI: 10.1063/1.1830489]

I. INTRODUCTION

The swirling motion of neutral fluids and plasmas is quantified by the vorticity, which can be viewed as the source function for the velocity field, in the same sense that an electric current is the source for a magnetic field. Vorticity is thus a primary physical quantity in equations for fluids and plasma dynamics. For quasi-two-dimensional velocity flow fields that occur in geophysical fluid dynamics (GFD) and in magnetized plasmas, it is essential to measure the vorticity field in order to understand quantitatively the dynamics of vortices and other coherent structures in the flow.^{1,2}

For quasi-two-dimensional flows, there is a scalar stream function whose Laplacian is the vorticity. In GFD the stream function is $\psi = gH(x, y, t)/f$, where $gH(x, y, t)$ is the gravitational potential energy in the height H of a column of neutral fluid and f is the Coriolis parameter from the rotation of the earth. In magnetized plasmas the stream function is $\psi = \varphi(x, y, t)/B$, where φ is the electrostatic potential and B is the ambient magnetic field strength. The fact that the plasma stream function is the electrostatic potential, which can be measured directly by suitable Langmuir probes, gives a unique advantage to the measurement of vorticity in plasmas over the measurement of vorticity in complex fluid dynamics. In neutral fluids, vorticity is constructed from velocity field measurements using particle image velocimetry,³ in which digital images of neutrally buoyant test particles (or seeds) in the fluid are processed with sophisticated computer

algorithms to infer the flow velocity, an expensive and somewhat complicated procedure that leads to significant levels of noise.

In this work we propose a different probe design for measuring directly the vorticity of the plasma motion. Fast digital measurements of the field aligned vorticity $\omega(x, y, t) = \nabla^2 \varphi / B$ can be measured with this vorticity probe. Here we describe the design of the vorticity probe and its use in a large steady-state cylindrical plasma in the large plasma device (LAPD).⁴ The experimental situation chosen is the one in which the Kelvin–Helmholtz instability is present due to a strongly localized radial electric field at the mid radius of the confinement vessel.

The vorticity probe measures both the dc and ac components of the vorticity with appropriate time filter. The principle of the vorticity probe is to use Langmuir probes in the stencil of the discretized Laplacian operator.

The experiments are performed in the upgraded LAPD⁴ at UCLA, which is an 18 m long, ≈ 1 m diameter magnetized plasma column created by a pulsed discharge from a barium oxide coated emissive cathode. The typical plasma parameters in LAPD are $n_e \sim 5 \times 10^{12}$ cm⁻³, $T_e \leq 15$ eV, $T_i \leq 1$ eV, $B < 0.2$ T with helium, argon, and neon as the working gas ($P_{\text{fill}} \sim 5 \times 10^{-5}$ Torr). Discharges in LAPD are typically fully ionized, but some residual neutrals may be present. We can get a conservative estimate of ion-neutral collisionality by assuming a neutral density equal to the density before ionization (consistent with the fill pressure at room temperature). This assumption yields a small ion-neutral collision frequency $\nu_{in} = n_0 v_i \sigma_{in} \sim 100$ /s. These collisions produce a very small background viscosity for the

^{a)}Electronic mail: horton@physics.utexas.edu

^{b)}Electronic mail: jcperez@physics.utexas.edu

^{c)}Electronic mail: tcarter@physics.ucla.edu

^{d)}Electronic mail: bengtson@physics.utexas.edu

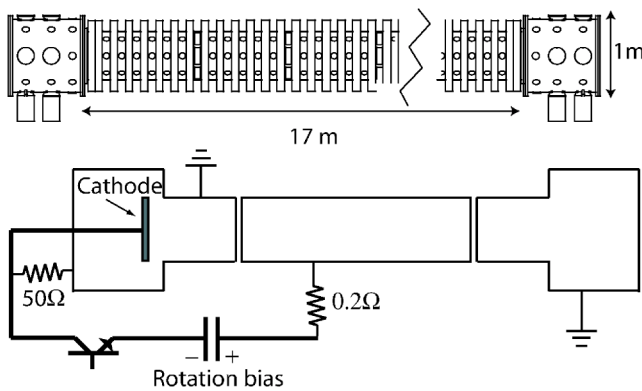


FIG. 1. Schematic of the large plasma device (LAPD), including a diagram of the circuit used for plasma column biasing.

plasma that is negligible for the wave numbers relevant to the fluctuations considered here. A drawing of the apparatus with a schematic of the discharge circuit and rotation biasing circuit are shown in Fig. 1.

This paper is organized as follows. In Sec. II we describe the design and application of the diagnostic instrument, called a vorticity probe (VP). In Sec. III we show some preliminary measurements obtained with the VP in the cylindrical LAPD plasma and we present probability distribution functions (PDF) for vorticity measurements that give evidence of long tail correlations in the shear layer. In Sec. IV we present linear and nonlinear simulations of the Kelvin–Helmholtz instability for comparison with the experimental data. Section V has conclusions.

II. THE VORTICITY PROBE

It is well known that the most natural quantity for describing eddies or vortices in neutral fluids or plasmas is the fluid vorticity, defined as

$$\boldsymbol{\omega} = \nabla \times \mathbf{v}. \tag{1}$$

This gives a local measure of the circulation of the velocity field at every point in the fluid plasma.

In the limit of a uniform magnetic field $B\hat{z}$ and with an electrostatic field $\mathbf{E} = -\nabla\phi(x, t)$, the ions and electrons move across the \mathbf{B} field with velocities

$$v_x = -\frac{1}{B} \frac{\partial\phi}{\partial y}(x, y, t), \tag{2}$$

$$v_y = \frac{1}{B} \frac{\partial\phi}{\partial x}(x, y, z, t). \tag{3}$$

The parallel component of the vorticity vector $\boldsymbol{\omega} = \nabla \times \mathbf{v}$ is given by

$$\omega = \frac{\partial v_y}{\partial x} - \frac{\partial v_x}{\partial y} = \frac{1}{B} \nabla_{\perp}^2 \phi(x, y, z, t). \tag{4}$$

To measure the vorticity we use the vorticity probe shown in Fig. 2. Then with the spacing $\Delta x = \Delta y = h$ of the four corners of the probe with respect to the center of the probe, we use the sum of the floating potentials of the corner minus four

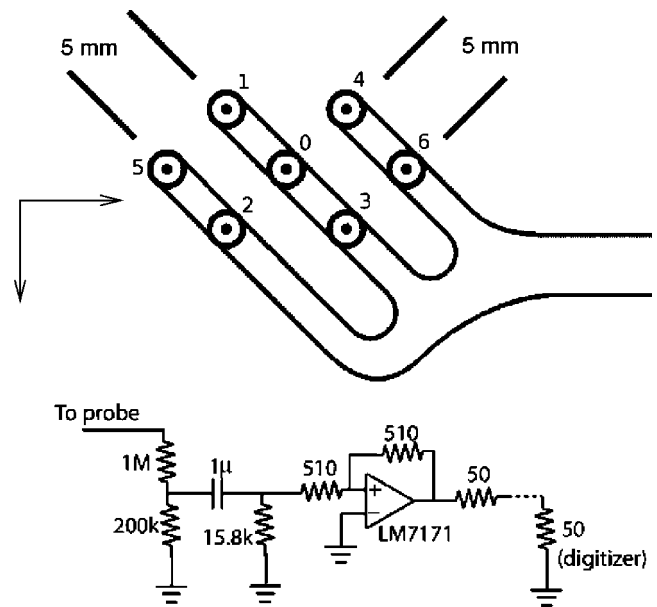


FIG. 2. Vorticity probe design. The probe is inserted into the LAPD plasma radially, so that the magnetic field is perpendicular to the surface of the probe tips.

times the floating potential at the center, $\phi_1 + \phi_2 + \phi_3 + \phi_4 - 4\phi_0$, to obtain the vorticity ω .

It is worth mentioning that the vorticity calculated in this way from the floating potential is valid as long as one assumes that the number of primary electrons at probe positions is small and that the temperature is the same at all probe tips. For the measurements we report here, these assumptions are justified given that the probe is introduced in the LAPD more than 10 m from the plasma source where the primary electrons are substantially reduced. Furthermore, measurements of temperature profiles show typical temperature scale length of the order of $L_{Te} \sim 100$ mm which is sufficiently greater than the probe tip distance $h = 5$ mm. If this were not the case, we would need to measure the temperature profile at each probe tip in order to get the plasma potential through the equation⁵

$$\phi_p(eV) = \phi_f(eV) + \frac{T_e}{2e} \ln\left(2\pi \frac{m_e}{m_i}\right) \tag{5}$$

$$= \phi_f(eV) - 3.5T_e \quad \text{for helium.} \tag{6}$$

The origin of the peaking of the electron temperature peak in the shear flow layer is not well understood, and suggests further research studies on the anomalous electron viscous heating.

This stencil is based on the finite difference approximation to $\nabla^2\phi$ given by

$$\nabla^2\phi = \frac{(\phi_{1,0} + \phi_{0,1} + \phi_{-1,0} + \phi_{0,-1} - 4\phi_{0,0})}{h^2}. \tag{7}$$

The vorticity is then given by dividing by the magnetic field B as in Eq. (4). The velocities into and out of the four sides of the square are also of interest. For the left-hand side, for example, the velocity is given by

$$v_x(\text{left}) = \frac{1}{B} \frac{(\varphi_1 - \varphi_2)}{2h}. \quad (8)$$

Clearly, the vorticity in Eq. (7) vanishes for $\varphi = C + Ax + By$. Only quadratic variations over the probe yield nonzero vorticity.

Just as in numerical simulations, the five-point sample of $\varphi(x, y, z, t)$ yields the true vorticity only for that part of the spectrum $\varphi(k_x, k_y, z, t)$ that has $k_x h < 1$ and $k_y h < 1$. Higher k modes yield an anomalous value for ω , although the value can still be interpreted unless $k_x h \gg 1$. For example, a mode with $k_x h = \pi$ and $k_y h = \pi$ leads to the value $-8\varphi_{0,0}/h^2$ for the right-hand side of Eq. (7).

The rate of convective transport of ω is given by

$$\frac{\partial \omega}{\partial t} + \mathbf{v} \cdot \nabla \omega = S_\omega(\mathbf{x}, t), \quad (9)$$

where the source/sink function S_ω includes various mechanisms that produce and absorb vorticity.

Since the $\mathbf{E} \times \mathbf{B}$ drift is incompressible for a uniform \mathbf{B} field, Eq. (9) also has the conservation form

$$\frac{\partial \omega}{\partial t} + \nabla \cdot (\omega \mathbf{v}) = S_\omega. \quad (10)$$

Averaging using Eq. (10) over the symmetry direction y (or θ) yields the transport equation

$$\frac{\partial}{\partial t} v'_y(x, t) + \frac{\partial}{\partial x} \langle \omega v_x \rangle = \bar{S}_\omega(x, t) \quad (11)$$

for the generation of sheared zonal flows $v'_y = d\langle v_y \rangle / dx$. It is worth noticing that the average flux of vorticity $\langle v_x \omega \rangle$ equals the divergence of the Reynolds stress $\langle v_x v_y \rangle$ per unit mass. Both the vorticity flux and the Reynolds stress can be measured by the vorticity probe.

In this experiment, the differential axial confinement of the electrons at the radius of the cathode controls the source of vorticity S_ω through the biasing of the cathode/anode with respect to the chamber walls. For tokamaks a similar E_r structure, usually an E_r well, is formed by the differential confinement of the ions at the edge of the plasma. This becomes a strong feature after the transition to the H mode.⁶

The vorticity probe was constructed from seven Tantalum tips as shown in Fig. 2. The tips are cylindrical, 0.02 inch in diameter, and 1 mm long. The tips are oriented along the direction of the magnetic field (into the page in Fig. 2). The Tantalum tips are held in alumina ceramics, which in turn are held by a stainless steel structure that is slotted in order to minimize perturbation to the plasma. The central five tips are arranged in a diamond pattern, with the outer four tips separated from the central tip by 5 mm. The five inner tips are used to measure the floating potential, which is then used to compute a finite-difference estimate of the vorticity, while the two outer tips allow measurement of the ion saturation current, in order to obtain the plasma density and radial particle flux $\langle nE_\theta \rangle / B$, as well as the Reynolds stress $nm_i \langle v_r v_\theta \rangle = (\rho / B^2) \langle E_r E_\theta \rangle$.

In order to compute the finite-difference estimate of the vorticity, four times the floating potential on the central tip

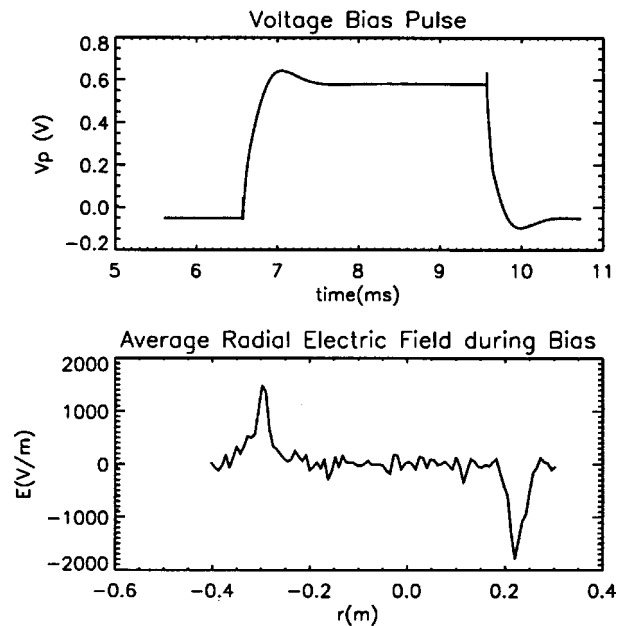


FIG. 3. Top: Typical cathode/anode bias voltage pulse with respect to the chamber wall for establishing the rotation jet. Bottom: Radial electric field measured in the stationary section of the bias pulse.

must be subtracted from the floating potential on the surrounding four tips. During biased rotation experiments in LAPD, the dc floating potential can reach values of the order of 200 V, substantially larger than the observed fluctuation amplitude (~ 1 V). The floating potential measurements are therefore performed using ac coupled amplifiers in order to reject the large low-frequency floating potential signal and to maximize the use of the dynamic range of the available digitizers. The amplifiers are constructed using wideband operational amplifiers (National Semiconductor LM7171) and flat response from 1 KHz to 10 MHz. A schematic of the measurement circuit is shown in Fig. 1. Data are acquired using 100 MS/s, 14 bit VME-based digitizers (eight channels per board, four available boards).

III. PROBE TEST ON THE KELVIN–HELMHOLTZ INSTABILITY

The Kelvin–Helmholtz instability is excited in the LAPD experiment by biasing the floating anode-cathode source with respect to the chamber wall of the device. This results in a sharply localized radial electric field as shown in Fig. 3. This electric field, along with the axial magnetic field, creates a sheared poloidal $\mathbf{E} \times \mathbf{B}$ jet stream at the edge of the plasma column. This jet stream flow seems to form as one of the natural self-organized states after the K - H instability in which the vorticity ω as a function of the potential φ , is a steady-state solution of the vorticity equation

$$\mathbf{v}_E \cdot \nabla \omega = 0. \quad (12)$$

Various types of solutions exist with or without embedded vortices. The simplest solution is a jet stream with localized $v_\theta(r)$. In Sec. IV B we show a nonlinear simulation that illustrates this feature.

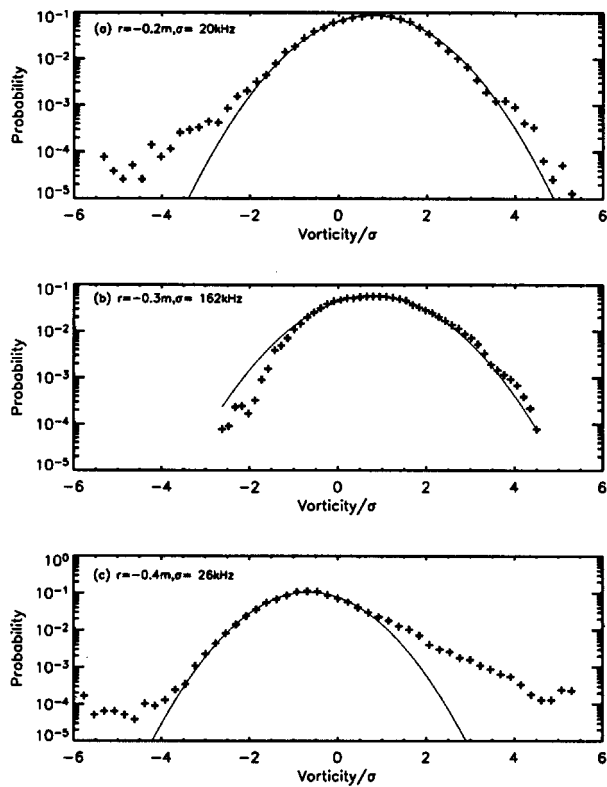


FIG. 4. Vorticity PDF for four radial position across the shear flow layer for the left-hand side ($r < 0$) of the plasma column. The sign of the excess vorticity counts over the Gaussian value switches from negative (counterclockwise rotation) to positive (clockwise rotation) in moving across the shear flow layer.

In Fig. 4 we show vorticity PDFs at representative points of the shear layer. In each plot we combine vorticity data from 25 similar shots, during 2 ms of the bias pulse between $t = 7.5$ ms and $t = 9.5$ ms, see Fig. 3. This corresponds to a total of 77 525 data points divided into 50 equally spaced bins of fluctuating vorticity amplitudes normalized to the standard deviation.

The heavy tails of the vorticity probability distribution functions shown in Fig. 4 signify that large values of the vorticity occur frequently. The situation here for vorticity fluctuations driven by the background plasma jet is similar to that of the density and density fluxes and the coherent intermittent structures measured in the linear PISCES-A⁷ and the ADITYA tokamak machine where the probability distributions showed heavy tails.⁸ This suggests that different studies with the vorticity probe may be useful for analyzing the edge turbulence of tokamaks, especially in the L–H mode transition.

In Fig. 5 we show relevant statistical quantities for an ensemble of 25 experimental runs under identical conditions. The measurements of vorticity show a high degree of reproducibility over the experiments. First, we consider the degree of correlation of the floating potential difference between the outermost probe pins five and six as the probe is scanned across the shear flow layer. The spacing between these probes is $d = 2\sqrt{25}$ mm = 14 mm. Frame (a) shows that the normalized correlation function $\langle \varphi_5 \varphi_6 \rangle$ is near unity except in the shear layer where it drops to about 0.7. Thus, we infer

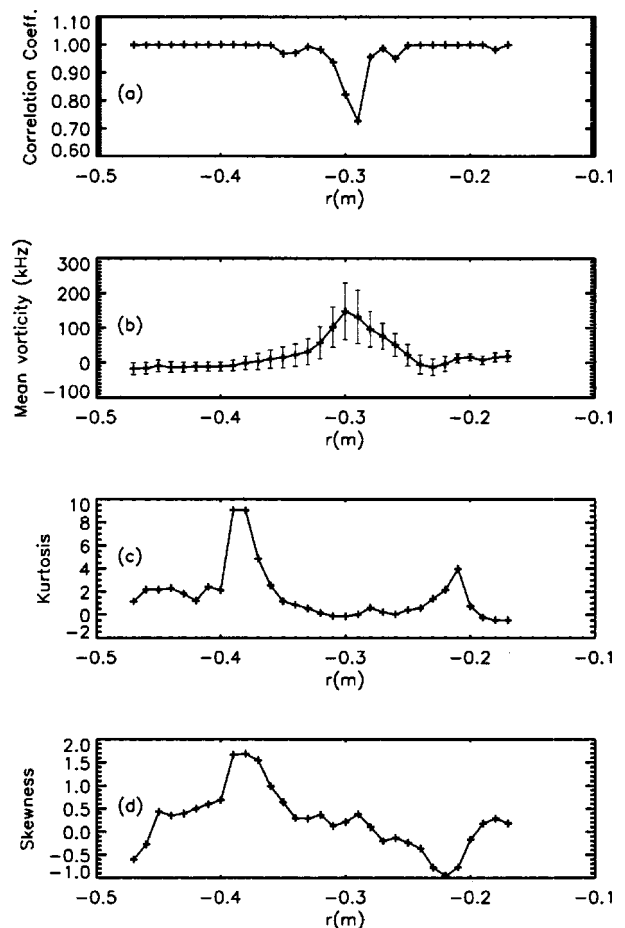


FIG. 5. Radial variation for the left-hand side of cylinder for the mean, the kurtosis, and skewness. The antisymmetry of the skewness agrees with the change if vortex rotation direction across the layer and coincides with the larger values of kurtosis that occurs in for a field of vortices.

that the radial correlation length of the fluctuations drops from greater than 14 mm to about 10 mm in the center of the shear flow layer.

Next we consider the vorticity mean values, as the probe is scanned along the radial direction, by averaging vorticity over time at each point in the shear layer and later averaging over the ensemble of the 25 experimental. Frame (b) of Fig. 5 shows the mean vorticity $\langle \omega \rangle$ as a function of the radius. From this plot, we see that the vorticity reaches a maximum value $\omega_{\max} = 150$ kHz, which is comparable to $v_{\max}/a \sim 10^4$ (m/s)/0.05 m ~ 200 kHz from the equilibrium radial electric field profile at $B = 0.075$ T. The positive core value agrees with the sign of chain of vortices expected from the KH instability.⁹

Frames (c) and (d) show that outside the core of the jet there is an intermittency of the vorticity probability distribution consistent with the heavy tails shown in Fig. 4. While the error bars on the mean vorticity suggest that it may be consistent to take the vorticity as vanishing outside the core of the jet stream, the small relative bias that is equal to the width of the error bar is such as to give vortices rotating counterclockwise outside the stream $r < -0.4$ m and clockwise inside the stream -0.4 m $< r < 0$ on the left-hand side of

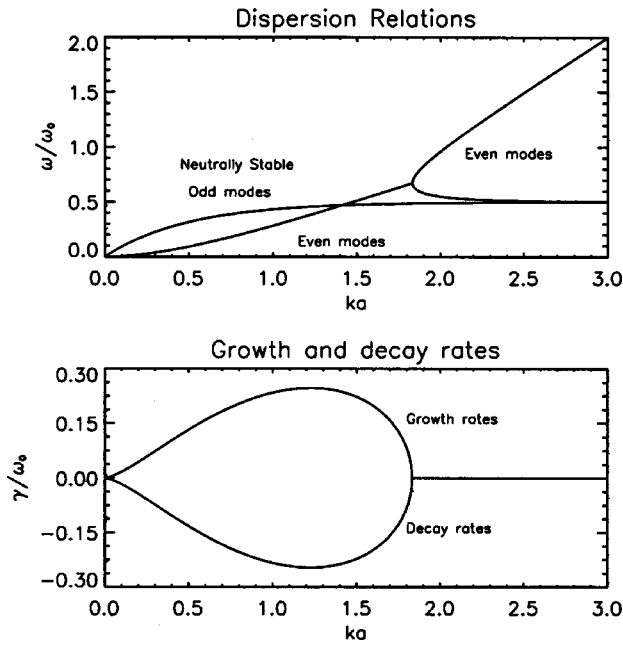


FIG. 6. Frequency and growth rate as a function of $k\rho_a$ for the model of the equilibrium radial electric field measured in the plasma. There are two modes: the unstable Kelvin-Helmholtz mode and the neutrally stable modes with odd symmetry corresponding to a wavy motion of the jet.

the cylinder. We will see in Sec. IV that the simulations show such a pattern of counter rotating vortices.

There are two types of aliasing errors: (i) the usual single probe sampling error for signal frequencies higher than the Nyquist $f_N = 1/2\delta t$ and (ii) spatial aliasing errors for short wavelength signals. For each pin there are antialiasing filters in frequency. This helps reduce spatial antialiasing under the assumption that small scale structures exist at higher frequency. The sample rate (and antialiasing filter) is at much higher frequency than the frequency of the observed fluctuations (we sample at a few MHz, and the fluctuations are at around 10–20 kHz). For spatial aliasing problem we consider the effect of the finite probe space h on a single wavelength signal, the ratio of vorticity measured with the probe to the actual value of vorticity is given by

$$R(\mathbf{k}, h) = 4 \frac{\sin^2\left(\frac{k_x h}{2}\right) + \sin^2\left(\frac{k_y h}{2}\right)}{h^2(k_x^2 + k_y^2)}. \quad (13)$$

For $kh < 1$ we have $R \approx 1$. For $k'_x = k_x + 2\pi n$, $k'_y = k_y + 2\pi m$, the probe picks up the same signal for \mathbf{k} and \mathbf{k}' which is the aliasing error. However, the probe value is smaller as given by $R(\mathbf{k}, h)$ at the spatial Nyquist frequency $k_N = \pi/h$ where the ratio function is $R = 4/\pi^2 \approx 0.444$. So, keeping data for $k < k_N \approx 628 \text{ m}^{-1}$ will largely suppress the aliasing errors. Using a range of probe sizes will allow an accurate assessment of the power in the high k components.

IV. SIMULATIONS

A. Linear simulation

In order to model the Kelvin-Helmholtz instability we consider the electrostatic response of the plasma in a two-

fluid model, where the dynamics for the electrostatic potential is obtained from conservation of charge under the assumption of quasineutrality, i.e.,

$$\nabla \cdot \mathbf{j} = 0. \quad (14)$$

Here $\mathbf{j} = \mathbf{j}_p$ is the polarization current,

$$\mathbf{j}_p = -\frac{m_i n_i}{B^2} \frac{d}{dt} \nabla \varphi = -\frac{m_i n_i}{B^2} \left(\frac{\partial}{\partial t} + \mathbf{v}_E \cdot \nabla \right) \nabla \varphi, \quad (15)$$

with

$$\mathbf{v}_E = \frac{\mathbf{E} \times \mathbf{B}}{B^2} = \frac{1}{B} \mathbf{e}_z \times \nabla \varphi. \quad (16)$$

Equation (14) becomes

$$\left(\frac{\partial}{\partial t} + \mathbf{v}_E \cdot \nabla \right) \nabla^2 \varphi = \frac{\partial}{\partial t} \nabla^2 \varphi + [\varphi, \nabla^2 \varphi] = 0, \quad (17)$$

where we have introduced the Poisson bracket between two two-dimensional functions f, g :

$$[f, g] \equiv \frac{\partial f}{\partial x} \frac{\partial g}{\partial y} - \frac{\partial f}{\partial y} \frac{\partial g}{\partial x}. \quad (18)$$

In the shear layer the scale length L_{n_e} is calculated from the profile of the mean ion saturation current giving $L_{n_e} \sim 15 \text{ cm}$ which is large enough to justify neglect the density gradients in the shear flow modeling. This scale length is $\approx 15\rho_i$, where $\rho_i = 3 \text{ mm}$.

The simple KH model used here has canceling electron and ion currents from the $\mathbf{E} \times \mathbf{B}$ motion. The vorticity equation (17) is the statement that the divergence of the cross field current vanishes.

Considering a slab approximation for this plasma we take x as the radial coordinate and y to be the periodic coordinate. We then linearize Eq. (17) around a steady-state poloidal flow like that in the LAPD plasma rotation. By doing so we obtain Rayleigh's eigenvalue equation as

$$\varphi_k''(x) - k^2 \varphi_k(x) - \frac{k v_y''(x)}{k v_y(x) - \omega} \varphi_k(x) = 0. \quad (19)$$

During the rotation bias pulse, the maximum velocity in the flow corresponds to an electric field $E \approx 1.5 \text{ kV/m}$ which occurs approximately at $r \approx 0.4 \text{ m}$. Taking the magnetic field to be $B = 0.075 \text{ T}$ along the z direction we obtain

$$v_{\max} = \frac{E}{B} \approx 2 \times 10^4 \text{ m/s}. \quad (20)$$

We solve the eigenvalue problem for an idealized triangular flow profile that resembles the equilibrium electric field profile in Fig. 3, i.e., having the form

$$v_y(x) = \begin{cases} 0 & x \leq -1 \\ (1 - |x|) & |x| \leq 1 \\ 0 & x \geq 1. \end{cases} \quad (21)$$

Here the velocity is normalized to v_{\max} and all lengths to $a = 0.1 \text{ m}$, corresponding to the half width of the shear layer.

Differentiation with respect to x gives

$$v_y''(x) = \delta(x + 1) - 2\delta(x) + \delta(x - 1). \tag{22}$$

Therefore the eigenfunctions obey the simple equation

$$\varphi_k''(x) - k^2\varphi_k(x) = 0, \tag{23}$$

except at the points $x=0, \pm 1$. The jet flow has a steep vorticity gradient, modeled boundary conditions, which can be derived by integrating Eq. (19) around the singular points. Doing so results in the three boundary conditions

$$\Delta[\varphi_k'(-1)] = -\frac{k}{\omega}\varphi_k(-1), \tag{24}$$

$$\Delta[\varphi_k'(0)] = -\frac{2k}{kv_0 - \omega}\varphi_k(0), \tag{25}$$

$$\Delta[\varphi_k'(1)] = -\frac{k}{\omega}\varphi_k(1), \tag{26}$$

where we have defined the operator

$$\Delta[f(x_0)] \equiv f(x_0^+) - f(x_0^-). \tag{27}$$

In practice, the profiles are continuous, but vary rapidly over a small scale δ . The jump conditions are well satisfied if $k\delta \ll 1$; for $k=m/r$ this is equivalent to $m \ll r/\delta$.

We can also see that Eq. (19) is invariant under the transformation $x \rightarrow -x$. This means that if $\varphi_k(x)$ is a solution to Eq. (19) with eigenvalue ω , then $\varphi_k(-x)$ is also a solution with the same eigenvalue. This fact allows us to find eigenfunctions with a definite parity. Let us first look for odd eigenfunctions, i.e., eigenfunctions such that $\varphi_k(x) = -\varphi_k(-x)$. The general solution to the Rayleigh equation, Eq. (19), in this case is of the form

$$\varphi_k^{\text{odd}}(x) = \begin{cases} Ae^{-k|x|} \operatorname{sgn}(x) & |x| > -1 \\ B \cosh(kx) \operatorname{sgn}(x) + C \sinh(kx) & |x| \leq 1, \end{cases} \tag{28}$$

where we have chosen the solution to decay at $x \rightarrow \pm\infty$. By using the matching conditions at the singular points, we obtain the dispersion relation

$$\omega_k = \frac{1}{2}(1 - e^{-2k}). \tag{29}$$

We thus see that all the odd modes are neutrally stable. These modes, however, are important in the nonlinear analysis.

Now we proceed to consider the even modes, which satisfy $\varphi_k(x) = \varphi_k(-x)$. The general solution to the Rayleigh equation in this case is

$$\varphi_k^{\text{even}}(x) = \begin{cases} Ae^{-k|x|} & |x| > 1 \\ B \cosh(kx) + C \sinh(k|x|) & |x| \leq 1. \end{cases} \tag{30}$$

Applying the conditions at the singular point we obtain

$$\omega_k = \frac{1}{4}[(2k + e^{2k} - 1) \pm \sqrt{G(k)}], \tag{31}$$

where

$$G(k) \equiv 9 - 10e^{-2k} - 12k + e^{-4k} - 4e^{-2k}k + 4k^2. \tag{32}$$

The function $G(k)$ is negative for $0 \leq k \leq k_c$, where $k_c \approx 1.833$. Hence, in this range, the eigenvalues are

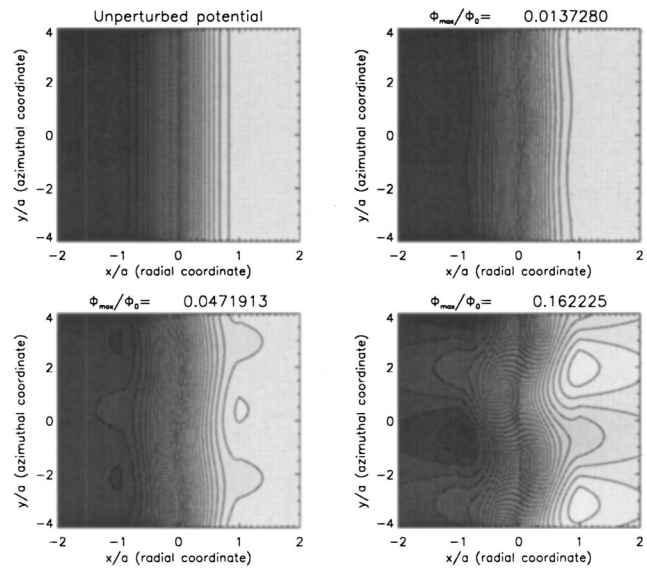


FIG. 7. Stream function $\psi = \phi/B$ from the isopotentials of the unstable eigenmode of Eq. (19). The last frame in the saturated state shows the alternation of the vortex directions across the jet.

$$\omega_{k\pm} = \omega_R \pm i\gamma_k, \tag{33}$$

where

$$\omega_R = \frac{1}{4}(2k + e^{2k} - 1), \tag{34}$$

$$\gamma_k = \frac{1}{4}\sqrt{-G(k)}. \tag{35}$$

In this case, modes with eigenvalue ω_{k+} are unstable and grow according to

$$|\varphi_k(x, t)| = |\varphi_k(x)|e^{\gamma_k t}. \tag{36}$$

On the other hand we see that for every growing mode there corresponds a damped mode, due to the Hamiltonian structure of the system, namely, modes with eigenvalue ω_{k-} . If we include dissipation from viscosity and resistivity, the Hamiltonian symplectic structure is broken. However, e dissipation is more important for the high k modes.

The general wave function is of the form

$$\varphi(x, y, t) = \varphi_0(x) + \operatorname{Re} \left[\sum_k e^{\gamma_k t} \varphi_k(x) e^{i(ky - \omega_k t)} \right]. \tag{37}$$

Within the range $0 \leq k \leq k_c$ we have the following frequencies and growth rates.

We see that the fastest growing mode corresponds to $m = 7$. Figure 7 shows some isolines of the total potential

$$\varphi(x, y, t) = \varphi_0(x) + \varphi_k(x, y, t), \tag{38}$$

where

$$\varphi_0(x) = \begin{cases} 0 & x \leq -1 \\ \frac{1}{2}x^2 + x + \frac{1}{2} & -1 \leq x \leq 0 \\ -\frac{1}{2}x^2 + x + \frac{1}{2} & 0 \leq x \leq 1 \\ 1 & x > 1 \end{cases} \tag{39}$$

is the basic flow stream function.

TABLE I. Linear KH eigenfrequencies.

Mode number m	ω_0 (kHz)	γ (ks ⁻¹)
1	5	13.6
2	18	33.3
3	36.8	52.8
4	59.7	70.1
5	85.6	84
6	113.5	93.7
7	143	98.4
8	173.6	97.4
9	205	89.1
10	237	69.4
11	273.7	0

In the turbulent flow layer there is a broad band of fluctuation frequencies that are difficult to associate with the linear eigenmode frequencies shown in Table I. We have computed the power spectrum of the floating potential and the vorticity for different time series $\Delta T = N_T \Delta t$ from $N_T = 256$ to 2048 and averaged the results of the spectra over the M ensembles defined by dividing the stationary section of the bias pulse into M records of length $N_T \Delta t$. The result shows a broad band frequency spectrum, where the power decreases as f^{-3} from $f_1 = 1/N_T \Delta t \sim 1$ kHz to $f_{\max} = \pi/\Delta t = 1.6$ MHz in the case where $N_T = 1024$. Thus, the bulk of the power is at the low-frequency end of the spectrum.

B. Nonlinear simulation

For the nonlinear simulation of the LAPD shear layer during the rotation bias pulse, we use a nonlinear pseudospectral code that uses Fourier decomposition in space to compute gradients and Poisson brackets in k space and adaptive fifth/sixth order Runge–Kutta method to advance the solution in k space. Then we transform the advanced solution back to configuration space. This code was implemented to have periodic boundary conditions in both x (radial) and y (poloidal) coordinates.^{10,11} There are two disadvantages in using the local periodic slab model for the simulation. First, the dc rotation through

$$\langle \omega \rangle = \frac{1}{r} \frac{\partial(rv_\theta)}{\partial r} = \frac{\partial v_\theta}{\partial r} + \frac{v_\theta}{r}.$$

The first gradient component is dominant for the profile and is about 200 kHz, while the second rotational frequency Ω , which is symmetric about the peak of the jet, is $\Omega = v_{\theta, \max}/r \sim 60$ kHz. The second disadvantage is that the radial boundary conditions are not periodic. However, we can still get some qualitatively important results by using the local potential shown in Fig. 8. The top frame of Fig. 8 shows the initial state in which opposite vortices are shed from the right- and left-hand sides of the jet, so that there is a definite skewness $\langle \omega^3 \rangle$ that changes sign across the layer as measured with the vorticity probe. After some time, the simulation shows that the average value of vorticity along the y direction of Fig. 8 tends to decrease at each x point due

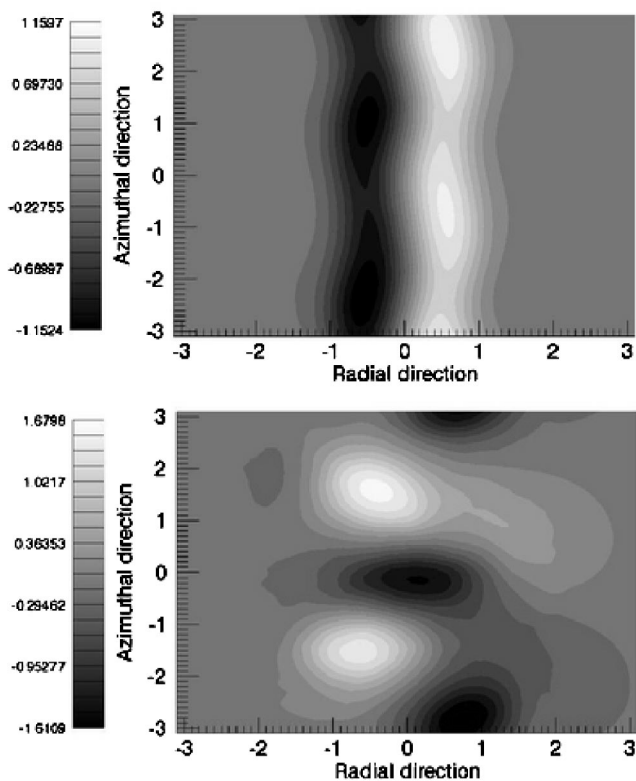


FIG. 8. The linear and nonlinear stages of the jets disassembly into positive and negative vortices. There is a coalescence of the vortices and a separation of the direction of rotations according to the direction of the jet. In the experiment the bias voltage maintains the vorticity injection which is transported away by the divergence of the Reynolds stress.

to the alternate counter rotating vortices lining up along the y direction. In both linear and nonlinear simulations, we have taken a slab of the rotating shear layer and therefore we have ignored the fact that the plasma is rotating as a whole, giving rise to a net background positive (clockwise when viewed into the magnetic field vector) vorticity associated to the equilibrium rotation. We believe this rotational vorticity explains the dominance of positive mean values in Fig. 5 and a peak at the center of about 150 kHz, where the flow velocity is maximum. Theoretical estimates give about 60 kHz for the background equilibrium vorticity, however, in the present experiment the floating potentials measured with the probe where high pass filtered at about ~ 1 kHz, so that part of the dc (equilibrium) potential gets through the filter giving rise to steeper gradients and hence higher values for the vorticity which could explain why the vorticity maximum is higher than expected.

The simple analytic model used in simulations takes the plasma density as constant over the shear layer. From the ion saturation current $I_{\text{sat}}(r)$ measured taken through a low pass filter, we know that just inside the shear flow layer there is a sharp increase of the electron density. In and outside the layer we find that $L_{ne} \sim 15$ cm which we argue is a sufficiently low gradient to neglect the $\delta n_e/n_e$ from $\mathbf{E} \times \mathbf{B}$ convection across the density gradient.

V. CONCLUSIONS

A probe design was presented that directly measures the vorticity field in plasma turbulence. The vorticity probe consists of five Langmuir probes in the stencil of the Laplacian with additional outer boundary probes for measurements of higher order phase gradients and propagation characteristics.

Construction of the vorticity probe was briefly described, and data obtained from measurements of an azimuthal flow jet $v_\theta(r) = -E_r/B$ in the LAPD experiment was presented.

The cross correlation signal across the probe shows that the pin signals are correlated and thus contain useful information rather than noise. The cross correlation drops from near unity to about 70% in the shear flow layer for the outermost pin tips separated by 14 mm, which is ≈ 20 ion gyroradii. The mean vorticity shows a large peak of $1.5 \times 10^5/s$ at the center and small residual positive and negative values of the order of $\pm 1 \times 10^4/s$ just outside the shear flow layer. The small residual values are just at the estimate of one standard deviation $\sigma_\omega(r)$ in the spread about the mean of the vorticity PDF. If we assume that the residual values of ω are statistically significant, then we see a confirmation of the odd symmetry of the sign of vorticity shed from the plasma jet.

A set of probes with different tip spacing would allow the collection of a relatively complete picture of the vorticity field from $\mathbf{E} \times \mathbf{B}$ flows in a magnetized plasma. In the future, we will integrate test particle motion and compare with tagged ions by the laser induced fluorescence technique to investigate the details of the transport across the plasma jet or E_r well.

The PDF of the vorticity were computed across the shear layer, as sampled at $\delta t = 0.3 \mu s$ over a steady-state period of $T = 2$ ms. The PDF shows strong tails in the regimes of maximum vorticity $v'_\theta = -E'_r/B$ near $r = -0.4$ m, where E_r is a maximum. These results are interpreted as showing the existence of a string of vortices of opposite signs on either side of the $E'_r = 0$ layer. The antisymmetric form of the skewness moment of the vorticity in Fig. 5 as well as the local peaks of the kurtosis function are consistent with a string of oppositely signed vortex chains on either side of the maximum of the $E_r(r)$ profile. This antisymmetric double chain of vortices was also studied with simple pseudospectral code simulation of the Kelvin–Helmholtz instability for their system parameters.

Other quantities available from the probe are the ion saturation current, for a measure of the plasma density and particle flux $\langle nE_\theta \rangle$ and the Reynold stress $nm_i \langle v_r v_\theta \rangle = (\rho/B^2) \langle E_r E_\theta \rangle$. Analysis of these fluxes will be presented in a future paper, along with a comparison to test particle transport in models for the measured fluctuations.

Plasma has the unique advantage over a neutral fluid in that the stream function for quasi-two-dimensional flow is the electric potential, which can be sensitively measured directly by electrical probes with standard Langmuir probe techniques. Vorticity in neutral fluids is inferred from particle image velocimetry of neutrally buoyant test particles in the flow. This measurement is a relatively complex procedure compared with the measurement by the vorticity probe and the image velocimetry is subject to high noise level when the vorticity is constructed from the measured velocity field.

The measurement of vorticity is of fundamental importance in theory of turbulent fluids and plasmas. Closure models lead to various relations for the probability distributions and moments of the vorticity. A classical neutral fluid example is the Proudman–Reid formula

$$\frac{d^2 \overline{\omega^2}}{dt^2} = \frac{1}{3} (\overline{\omega^2})^2$$

discussed in detail in Ref. 12 where this model is compared with that of Millionshchikov and Betchov. Developing the vorticity probe for plasma should provide new insight into plasma turbulence modeling.

ACKNOWLEDGMENTS

The authors thank J.E. Maggs, R.J. Taylor, and P. Pribyl for assistance with the biased rotation experiments on LAPD and M. Fassler for technical assistance in the construction of the vorticity probe.

The work was supported under the U.S. Department of Energy Contract No. DE-FG02-04ER 54742. Experimental work was performed at the UCLA Basic Plasma Science Facility which is funded by NSF and DOE.

¹A. Maurel and P. Petitjeans, *Proceedings of Vortex Structure and Dynamics, Workshop, Rouen, France* (Springer, Berlin, 1999).

²W. Horton and Y.-H. Ichikawa, *Chaos and Structures in Nonlinear Plasmas* (World Scientific, Singapore, 2000).

³C. E. Willert and M. Gharib, *Exp. Therm. Fluid Sci.* **20**, 181 (1991).

⁴W. Gekeleman, H. Pfister, Z. Lucky, J. Bamber, D. Leneman, and J. Maggs, *Rev. Sci. Instrum.* **62**, 2875 (1991).

⁵P. C. Stangeby, *J. Nucl. Mater.* **121**, 36 (1984).

⁶K. H. Burrell, *Phys. Plasmas* **4**, 1499 (1997).

⁷G. Y. Antar, *Phys. Plasmas* **10**, 3629 (2003).

⁸ADITYA Team, R. Jha, P. K. Kwa, S. K. Mattoo, C. V. S. Rao, and Y. C. Saxena, *Phys. Rev. Lett.* **69**, 1375 (1992).

⁹W. Horton, T. Tajima, and T. Kamimura, *Phys. Fluids* **30**, 3485 (1987).

¹⁰T. Tajima, W. Horton, P. J. Morrison, J. Schutkeker, T. Kamimura, K. Mima, and Y. Abe, *Phys. Fluids B* **3**, 938 (1991).

¹¹W. Horton, *Phys. Fluids B* **1**, 524 (1989).

¹²A. S. Monin and A. M. Yaglom, *Statistical Fluid Mechanics* (MIT, Cambridge, MA, 1965).